ON THE DAMAGE MECHANISMS IN A CONTINUOUS CASTING MOLD: AFTER-SERVICE MATERIAL CHARACTERIZATION AND FINITE ELEMENT SIMULATION

Jelena Srnec Novak[a,*], Alex Lanzutti[a], Denis Benasciutti[b], Francesco De Bona[a], Luciano Moro[a], Andrea De Luca[c]

[a] Dipartimento Politecnico di Ingegneria e Architettura (DPIA), University of Udine, via delle Scienze 208, 33100, Udine, Italy. E-mails: jelena.srnec@uniud.it, alex.lanzutti@uniud.it, francesco.debona@uniud.it, luciano.moro@uniud.it

[b] Department of Engineering, University of Ferrara, via Saragat 1, 44122, Ferrara, Italy. E-mail: denis.benasciutti@unife.it

[c] Danieli Research Center, via Nazionale 41, Buttrio (UD) 33042, Italy. E-mail: a.deluca@danieli.it

Abstract

A mold is a part of a continuous casting plant where the molten steel starts to solidify. The inner surface of the mold undergoes a cyclic thermal load. In fact, service conditions are characterized by a high thermal flux, which vanishes when the plant is switched off. The highest temperatures occur in the area just beneath the free level of liquid steel (meniscus). The same area is typically characterized by thermal fatigue cracks when the mold is inspected after service.

* Corresponding author.
E-mail: jelena.srnec@uniud.it
Phone: +39 0432 558297
Fax: +39 0432 558251

This work presents the characterization of the material of a copper mold after it had been used in the plant. The aim was to understand the damage and cracking mechanism, and our analysis confirmed that a network of cracks was present on the inner mold surface in the meniscus area, which experienced the maximum temperature gradients. Metallurgical examination demonstrated the transgranular characteristics of cracks, thus suggesting that thermal fatigue was the main cause of the damage observed. The location of the thermal fatigue cracks corresponded to the area experiencing the highest levels of plastic strains, as confirmed by the results of a finite element analysis simulating the mold in-service conditions.

Keywords

Metallurgical examination, Failure analysis, Degradation, Thermal fatigue, Finite element analysis

1. Introduction

In continuous casting, the molten steel flows from a tundish into a mold, where it starts to solidify. The mold is thus a key component of the overall casting process, as it is subjected to high thermal loads and it also controls the initial shape and quality of semi-finished products (e.g. billets, blooms, slabs), before they enter the rolling mill lines [1-3].

The mold is essentially a water-cooled hollow tube with a rectangular or round cross section. It is usually made of copper alloy which facilitates an optimal combination of thermal and mechanical properties [3-10]. The inner surface of the mold is coated with nickel or chromium-based plating to protect the substrate underneath [11-13].

When the casting plant is operating, a huge thermal flux q is transferred from the molten steel, which is in contact with the inner mold surface, to the water-cooled outer side of the mold (Fig 1). The values of this flux vary between two conditions: q=0 when the plant is switched off, q=q_{max} when the plant is switched on and has reached full capacity, (Fig 2). The mold is exposed, on its inner surface, to a high time-varying temperature combined with a high thermal gradient across the mold wall. This cyclic thermal loading promotes thermal fatigue cracks in the meniscus area, which is the most thermally-stressed and strained region of the mold.

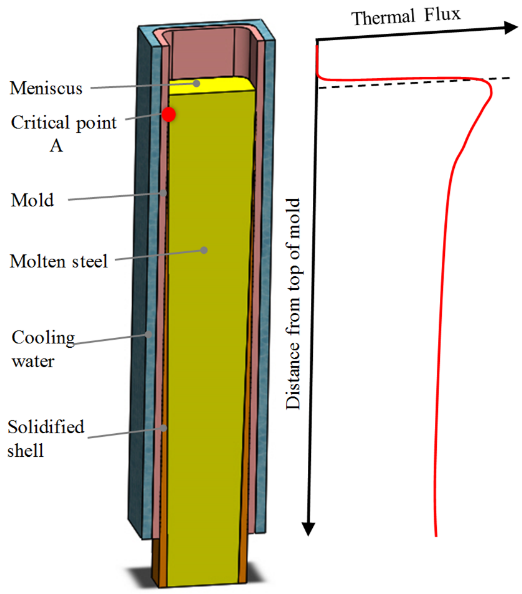

Fig. 1. A mold under working conditions (half section) and axial thermal flux distribution when $q=q_{max}$.

A mold without cracks ensures safety during the working process and guarantees the quality of the final product [1, 3]. On the other hand, through-thickness cracks must be avoided as any contact between cooling water and molten steel would have catastrophic consequences.

Several metallurgical studies [2, 8, 11-13] have been performed to determine the complex damage mechanism that occurs in the mold during its service life. Faries *et al.* [12] observed crack propagation through the copper substrate with a depth ranging from 0.6 mm to 5 mm. All cracks were found within the area approximately 100÷140 mm from the top of the mold (i.e. 0÷40 mm below the meniscus position). The same observations were reported by [2, 8, 11] for square and funnel molds.

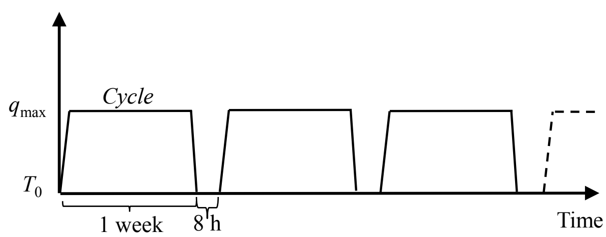

Fig. 2. Variation of the thermal flux during the service life of a mold.

The mold in the meniscus zone is damaged because of a detachment of the coating material and mechanical degradation assisted by the chemical attack of low melting point elements on the Cu substrate which thus becomes embrittled [1, 2]. The coatings are used to cover the internal walls of the mold, and they are affected by a thermo-mechanical degradation that reduces the mechanical properties of the deposit [8, 14].

The inner surface of the mold undergoes high fluctuating thermal stresses, which can lead to thermal fatigue. In order to better understand the source of the crack formation and thus to enhance the component service life, we investigated a possible correlation between the metallurgical observations and the stress and strain distribution in the cracked area. This work first presents a metallurgical investigation of a copper mold, and then details the results of a thermo-mechanical analysis performed with numerical techniques.

2. Experimental and numerical procedure

2.1 Sample extraction and microstructural characterization

A copper mold with length 1000 mm, rectangular cross section (172 x 174 mm) and thickness 15 mm (see Fig. 3), internally coated with a thin layer of hard Cr, was investigated at the end of its service life. The copper alloy of the mold had a chemical composition equal to a C14700 alloy, according to ASTM B124B standard [15], see Table 1.

Table 1. Chemical composition of the mold alloy (wt%).

Cu+Ag	P	S
Bal.	0.004	0.3

First, the copper mold was visually inspected to locate the most damaged areas, from which samples were subsequently extracted. As illustrated in Fig. 3a, the area near the meniscus is characterized by a wide network of cracks, while the surrounding parts seem to be unaltered.

To characterize the mold microstructure and to determine how cracking takes place, metallurgical investigations (light microscope and SEM) were performed on a total of five samples extracted from different areas of interest. Two metallographic samples (A1 and A01) were taken from the meniscus area (labeled A in Fig. 3b), one from the surface center, and one from the corner, respectively. Furthermore, in order to have a complete overview of the degradation mechanisms that took place in the mold, three samples were taken from regions outside the meniscus zone (labels B1, C1, D1). The samples used for microstructural investigation are presented with white squares in Fig. 3b.

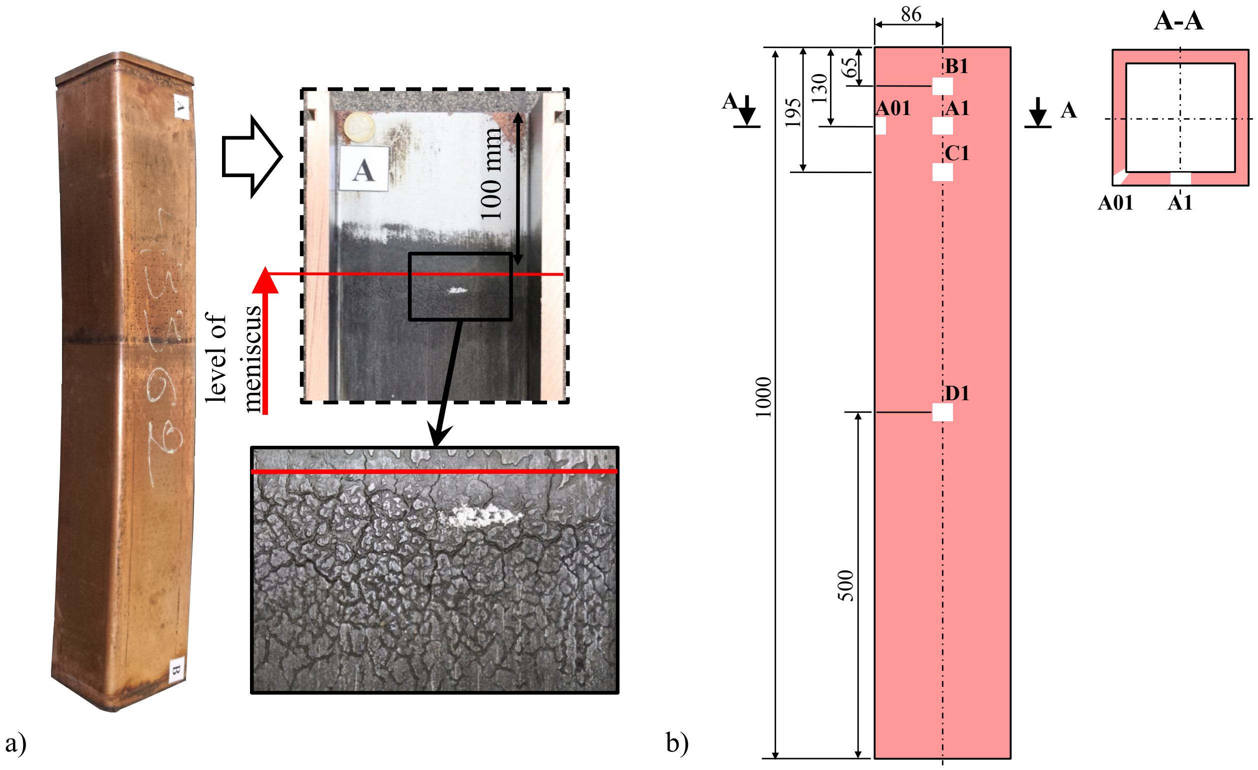

Fig. 3. Mold under investigation with damaged inner surface (a), positions of extracted samples (b).

The samples for the metallurgical investigation were extracted from the mold using a refrigerated abrasive wheel. Each sample underwent metallographic preparation (embedded in epoxy resin, ground with SiC papers and refrigerated with water, and then polished using fabric discs wetted with diamond suspension) in order to obtain a mirror-like surface.

Before the metallographic preparation, polished samples were analyzed by SEM, in both the cross section and the top view (orthogonal and parallel to the original free surface of the mold) to determine the degradation mechanisms in each zone of the mold (in the case of samples A01, only the cross section). The same samples were etched, using a solution of $H_2O:NH_3:H_2O_2=1:1:1$, and then analyzed by a light microscope to assess the crack morphology, the grain size (intercept method), and microstructure. Finally, the samples were analyzed by a stereoscope to identify the crack density (top view) and the average crack depth. The analyses were performed using the intercept method on the specimens extracted at different positions along the mold height (samples A01, A1, B1, C1, D1). On the same samples, Vickers micro-hardness profiles were acquired from the external surface to the core of the mold wall.

One specimen was used to measure the chemical composition of the alloy by means of Rf glow discharge optical emission spectrometry (Rf-GDOES), which was calibrated for bulk analysis of Cu alloys.

2.2 Numerical simulations

The thermal stress distribution occurring in the mold was studied with a thermo-mechanical analysis [4-7]. A three dimensional (3D) finite element model was required, due to the non-uniform distribution of the thermal flux through the mold length. Since the component has two planes of symmetry and is symmetrically loaded, only a ¼ model with suitable symmetry boundary conditions was considered in the analysis. The mesh was refined close to the meniscus where the maximum thermal gradient is expected, see Fig. 4.

A thermal analysis was performed with an 8-node brick thermal element. The thermal problem is quite complex as, in principle, it would be necessary to take into account the fluid dynamics of the molten steel (whose temperature is around 1500 °C), and also the presence of a gap between the steel and mold, which is filled with air and mold lubricant that acts as an insulating barrier.

In this study, the thermal analysis was performed according to the usual simplified procedure [1-3], where a thermal flux was imposed on the inner surface, while convection was considered on the outer surface of the mold to simulate water cooling. The red line in Fig. 1 shows the trend of the thermal flux adopted in the analysis, which was estimated according to the mathematical formulation proposed in [16] and then calibrated with experimental measurements. The temperature of the cooling water was 40 °C and the convection coefficient was 48000 W/m^2K. The convection coefficient was obtained according to the procedure described in [17]. Thermal conductivity was

377 W/mK at room temperature and 370 W/mK at 100 ^{o}C or above. The time-variation of the thermal flux from the plant start-up phase to the working condition (and vice versa) was simulated by a sequence of steady state analyses. In fact, this variation occurs over a relatively short time interval (minutes) compared to the total length of a whole cycle (days). A nonlinear solution was carried out to simulate the temperature dependence of thermal properties.

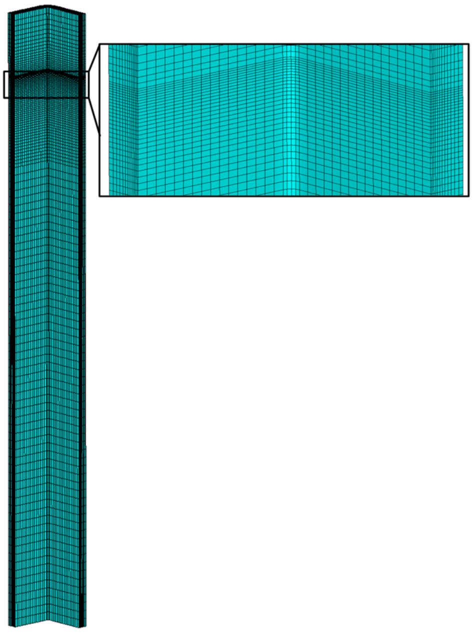

Fig. 4. Finite element model.

The temperature distribution calculated previously in the thermal analysis was the input data for the subsequent mechanical simulation, where structural elements with eight nodes were used. Since the real component is supported by four slots in the upper part, it can be considered free to expand. Therefore, no mechanical constraints need to be defined in the finite element model. As a result, the calculated stress-strain distribution only depends on the temperature distribution in the model. In line with [18], the mechanical load induced by the ferrostatic pressure was not considered. The dependence of the material parameters on the temperature was also taken into consideration.

With respect to earlier studies [1, 17] that used overly simplified material models (bilinear kinematic), this study adopted a combined nonlinear kinematic-isotropic material model, whose parameters were estimated from experimental data under cyclic loading at three temperature levels [9, 19]. The combined kinematic-isotropic model is able to represent simultaneously the Bauschinger effect and the cyclic hardening/softening behavior of a material. The von Mises yield criterion can be represented as [20]:

$$\sqrt{\frac{3}{2}(\boldsymbol{S}-\boldsymbol{X}):(\boldsymbol{S}-\boldsymbol{X})}-R-\sigma_0=0 \tag{1}$$

where $\boldsymbol{S}$ is the deviatoric stress tensor, $\boldsymbol{X}$ is the back stress tensor, R is the drag stress and σ_0 is the initial yield stress. In this case, the yield surface both translates (controlled by $\boldsymbol{X}$) and expands (controlled by R) with the plastic strain ε_p. In the literature, several kinematic models have been proposed [20]. The Chaboche model (nonlinear kinematic) assumes that the increment in the back stress d$\boldsymbol{X}$ is expressed as a function of the plastic strain increment $d\varepsilon_{pl}$ and the accumulated plastic strain $d\varepsilon_{pl,acc}$ [20]:

$$\boldsymbol{X}=\sum_{i=1}^{n}\boldsymbol{X}_i \quad ; \quad d\boldsymbol{X}_i=\frac{2}{3}C_i d\boldsymbol{\varepsilon}_{pl}-\gamma_i\boldsymbol{X}_i d\varepsilon_{pl,acc} \tag{2}$$

where C is the hardening modulus, and γ is the non-linear recovery parameter. The nonlinear isotropic model controls the homothetic expansion of the yield surface [20]:

$$dR=b(R_\infty-R)d\varepsilon_{pl,acc} \tag{3}$$

where R_∞ is the saturated drag stress and b controls the speed of stabilization. Material parameters adopted for mechanical simulation are presented in Table 2.

Table 2. Material properties for C14700 [9, 19].

Temp. (ºC)	E (MPa)	σ_0 (MPa)	C_1 (MPa)	γ_1	C_2 (MPa)	γ_2	C_3 (MPa)	γ_3	R_∞ (MPa)	b
20	119988	113	25880	1627	24460	1624	15620	315.4	-68	2.352
250	106080	110	31310	1708	10240	343.6	5256	1748	-75	3.894
300	103800	108	13170	1092	10700	398.2	10650	1155	-77	5.293

This combined plasticity model is particularly suitable for thermal fatigue analyses as it enables the stress evolution over cycles to be accurately calculated. The copper alloy considered in this study showed a typical softening behavior over cycles, with the yield stress decreasing as the accumulated plastic deformation increased.

3. Results

3.1 Microstructural characterization

Visual inspection revealed that the mold was heavily damaged in the meniscus area, as indicated in Fig. 3a. A closer examination of the mold inner surface showed that a web of cracks was formed in the area within 100 ÷ 140 mm from the top of the mold, i.e. beneath the level of the maximum thermal flux. In this location, the surface of the mold generally reaches the highest temperatures. Indeed, in this area the copper mold is in contact with the molten metal at high temperature, as indicated in Fig. 1. Representative SEM images of the samples A01, A1, B1, C1 and D1 are shown in Fig. 5 and Fig. 6. As highlighted in Fig. 5, the mold underwent a degradation mechanism linked to the cracking of the protective coating layer, which was completely detached in samples A01 and A1 (samples extracted in the most thermally-stressed region). In the same region, a thick layer of altered material was formed in the substrate.

The EDXS analyses, see Table 3, showed that the Cu substrate was converted into a brass with a Cu/Zn weight ratio between 0.5 and 1, which corresponds to the formation of β' (ratio close to 1) and γ (ratio close to 0.5) brittle phases or a mixture of the two [2, 21, 22]. These phases were full of cracks, mostly in samples A01 and A1. In sample A1 the crack passed through the brass and continued in the underlying copper substrate. The crack was surrounded by another phase composed of Zn, S and Pb.

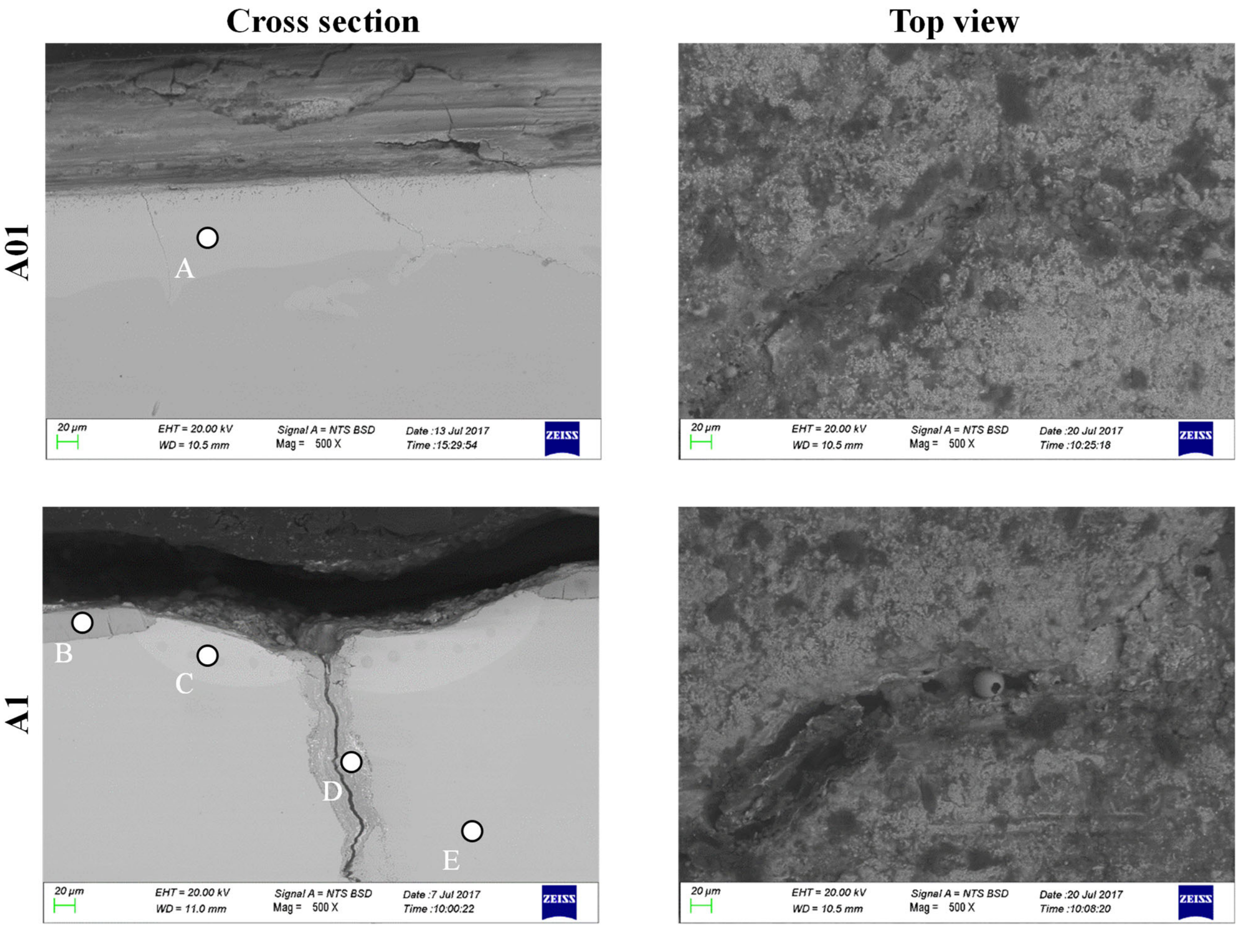

Fig. 5. SEM analysis of samples A01, A1 (top view and cross section). The letters indicate the areas analyzed by EDXS.

Samples B1 and C1, which are close to the meniscus area, presented a heavily damaged coating, while the Cu material underneath was only slightly affected by chemical degradation, which was the most pronounced in sample C1 (arrow), see Fig. 6. The detailed SEM analysis in sample C1 showed the infiltration of low melting point elements through the cracks of the coating, see Fig. 7 and Table 4. These elements reached the Cu substrate and reacted with it, producing a reaction layer.

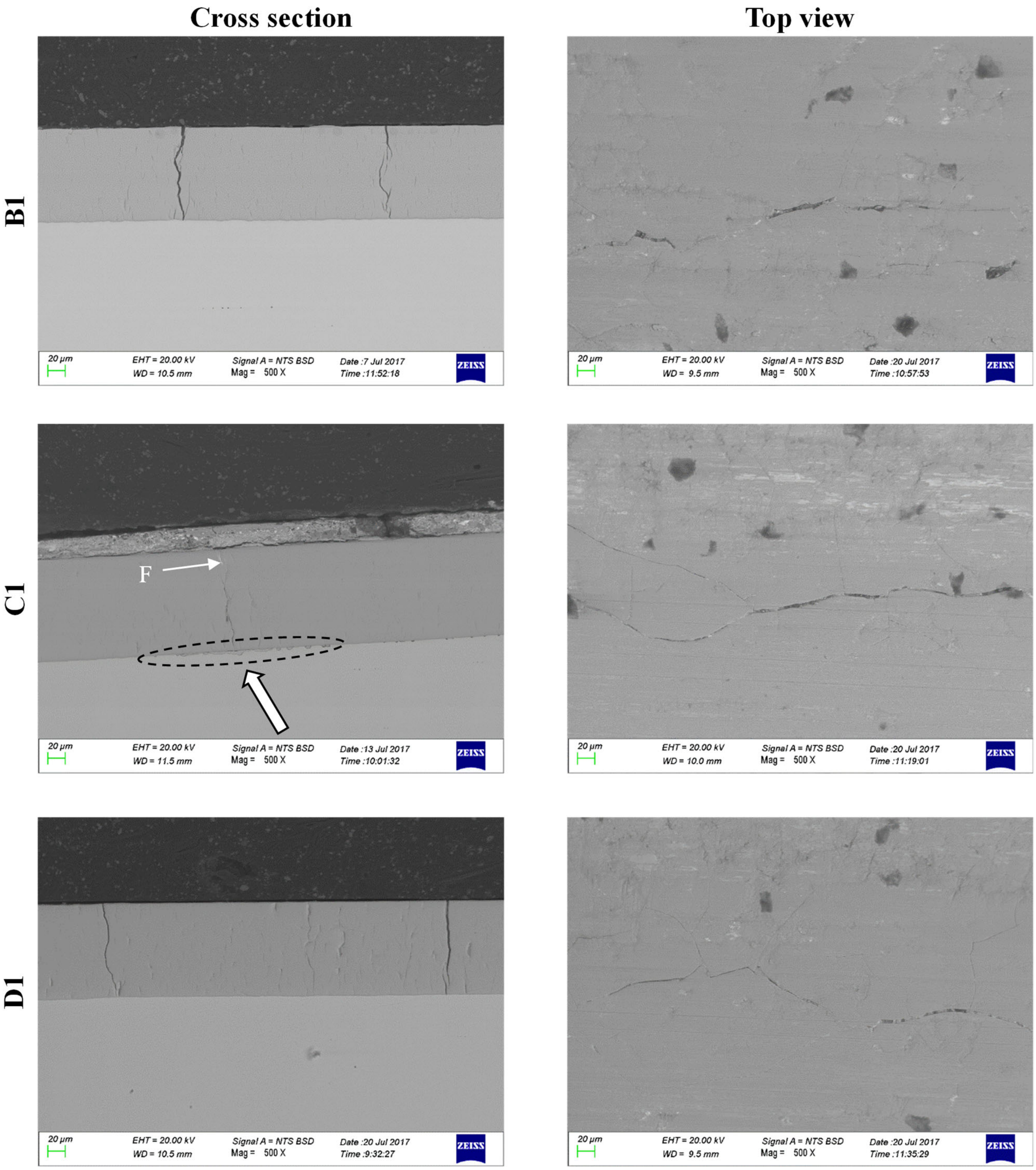

Fig. 6. SEM analysis of the samples B1, C1, D1 (top view and cross section). The letters indicate the areas analyzed by EDXS.

Table 3. Semi-quantitative results in weight percentage (wt%) obtained by EDXS analysis in areas highlighted in Fig. 5 and Fig. 6.

Zone under investigation	wt%	S	Mn	Fe	Cu	Zn	Pb	Cr
A					Bal.	66.00		
B					Bal.	62.04		
C					Bal.	65.14		
D		22.04	9.14	1.12	Bal.	20.51	3.20	
E					Bal.			
F		14.83			Bal.		69.24	12.70

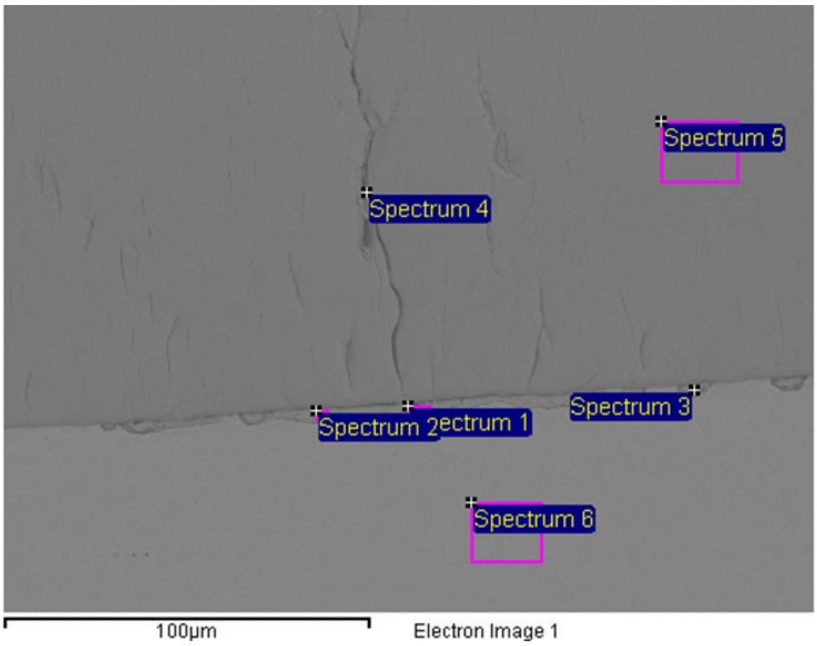

Fig. 7. Detail of the interface of sample C1 (circled area in Fig. 6).

Table 4. Semi-quantitative results in weight percentage (wt%) obtained by EDXS analysis in areas highlighted in Fig. 7.

Zone under investigation	wt%	S	Cr	Mn	Fe	Cu
Spectrum 1		20.32	3.19			Bal.
Spectrum 2		19.68	4.46			Bal.
Spectrum 3		18.66	3.45	1.74	2.11	Bal.
Spectrum 4			97.50	1.55		Bal.
Spectrum 5			98.19	1.81		Bal.
Spectrum 6						Bal.

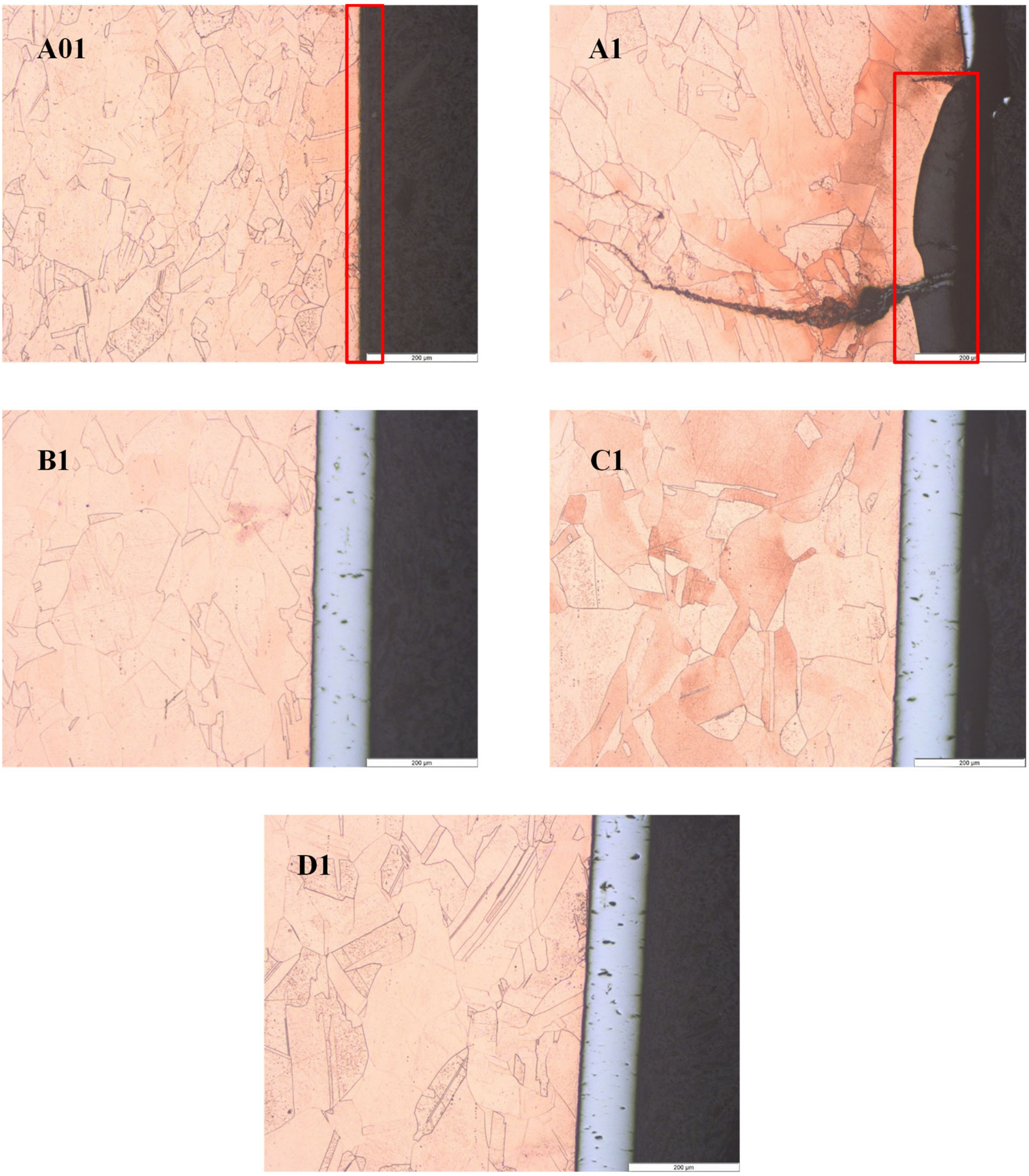

Fig. 8. Microstructural characterization of the analyzed samples.

The microstructure of samples A01, A1, B1, C1, D1 is shown in Fig. 8. As already observed by the SEM analysis, the light microscopy results confirmed that the mold surface was composed of a Cu substrate coated with a layer of hard chromium (0.1 mm thickness). The coating showed many micro cracks and had almost been completely removed in the specimens extracted from the meniscus area (A01 and A1). The microstructure of the substrate was composed of austenitic grains in the bulk material (range: ~70±30 µm). The grains seem to be coarser in specimen A1 compared to the other samples. Specimens B1, C1, D1 did not show any microstructural difference between the core and surface. In addition, samples A01 and A1 presented a surface layer that reacted with the molten metal (indicated in Figs. 5, 8 and analyzed previously by EDXS), and some cracks that nucleated in the external reacted layer and propagated to the Cu substrate. The cracks were sharp with transgranular propagation, and contoured with a slight reaction layer that was previously identified by SEM analysis (Fig. 5 point D). The morphology of the crack nucleation was barely visible under a light microscope. The SEM analysis of the material surface (Fig. 9) showed an intergranular crack nucleation in proximity of the surface that had reacted with molten metal. In this region, the material presented some intergranular morphologies/phases (black arrows) that were likely to reduce the material toughness locally.

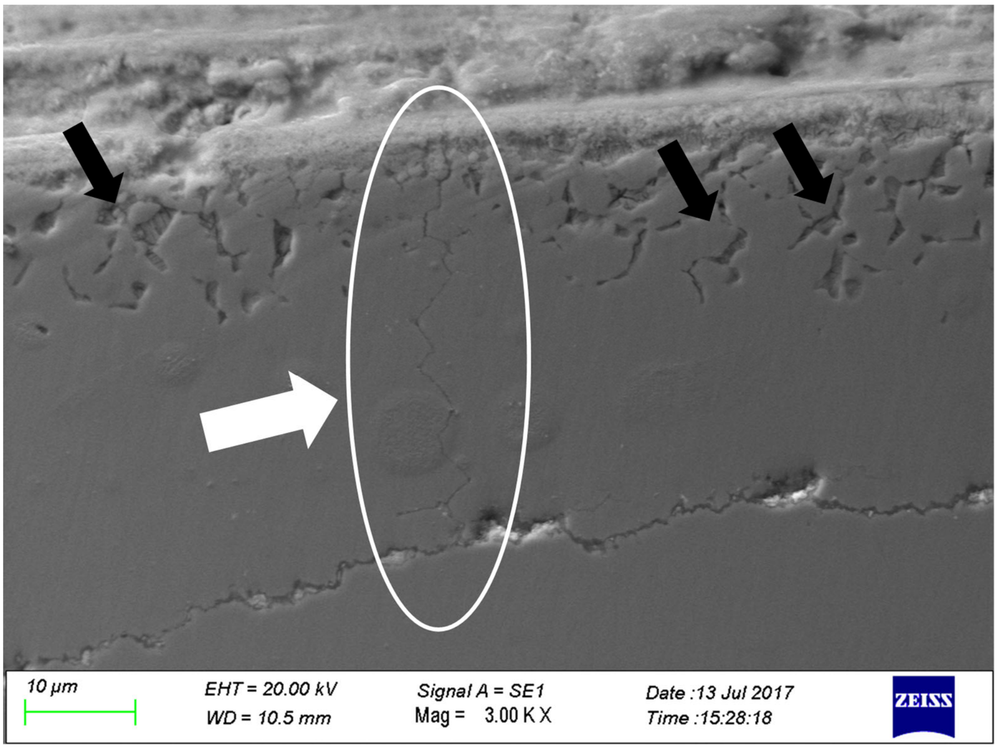

Fig. 9. Detail of the material surface that identifies the crack nucleation morphology. The black arrows indicate the intergranular features. The white circle indicates the intergranular fracture.

The samples extracted in proximity of the meniscus showed several transgranular cracks, as also highlighted by the microstructural examination. In the meniscus area, the average crack density and average crack depth were 0.3 cracks/mm and 2.8 mm, respectively, in both directions (longitudinal and transversal with respect to the mold axis). An example of the crack length and morphology, obtained from sample A1, is shown in Fig. 10.

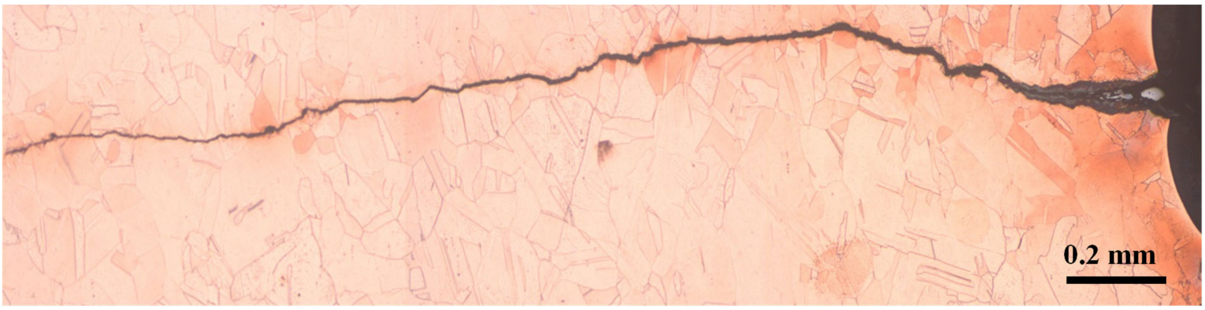

Fig. 10. Image of the crack extension in sample A1.

The crack was almost transgranular when it proceeded in the bulk material. The transgranular shape was maintained in all its length.

The micro-hardness profiles are shown in Fig. 11. As highlighted by Fig. 11a, the hardness was higher in proximity of the surface because of the presence of a hard chromium coating (samples B1, C1, D1) or due to the γ Cu-Zn phase (samples A01, A1). On the other hand, the hardness of the substrate was constant for all the analyzed samples. Only specimen A1, which was extracted from the center of the mold surface in the meniscus area, presented a lower hardness value up to a depth of 1-2 mm. These results agreed with the microstructural material characterization that exhibited a coarser microstructure in sample A1 compared to the others.

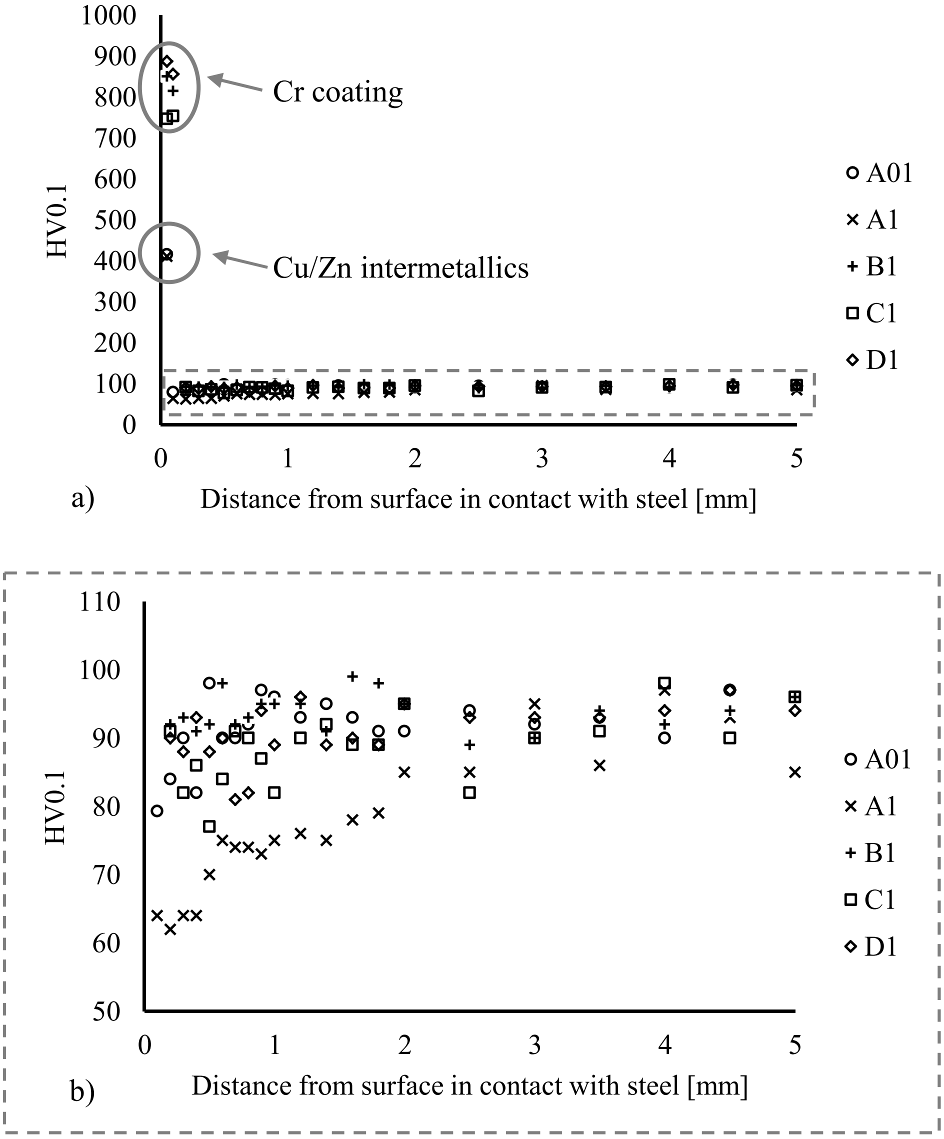

Fig. 11. Micro-hardness profiles for the tested specimens: a) complete profile, b) zoom of the hardness between 50 and110 HV0.1 (square area of Fig. 11a).

3.2 Thermo-mechanical results

The temperature distribution obtained at the maximum thermal flux is presented in Fig. 12a. The highest temperature was observed at 30 mm below the position where the maximum flux was applied, at the point labeled with the letter “A”, where the largest through-thickness thermal gradient also occurred.

The von Mises stress distribution is shown in Fig. 12b. The stresses also exceeded the yield stress in those regions of the inner mold surface in which the thermal flux attained its largest values. This is also evidenced in Fig. 12c, which displays the von Mises plastic strain distribution. The maximum plastic strains were located where the highest temperature occurred.

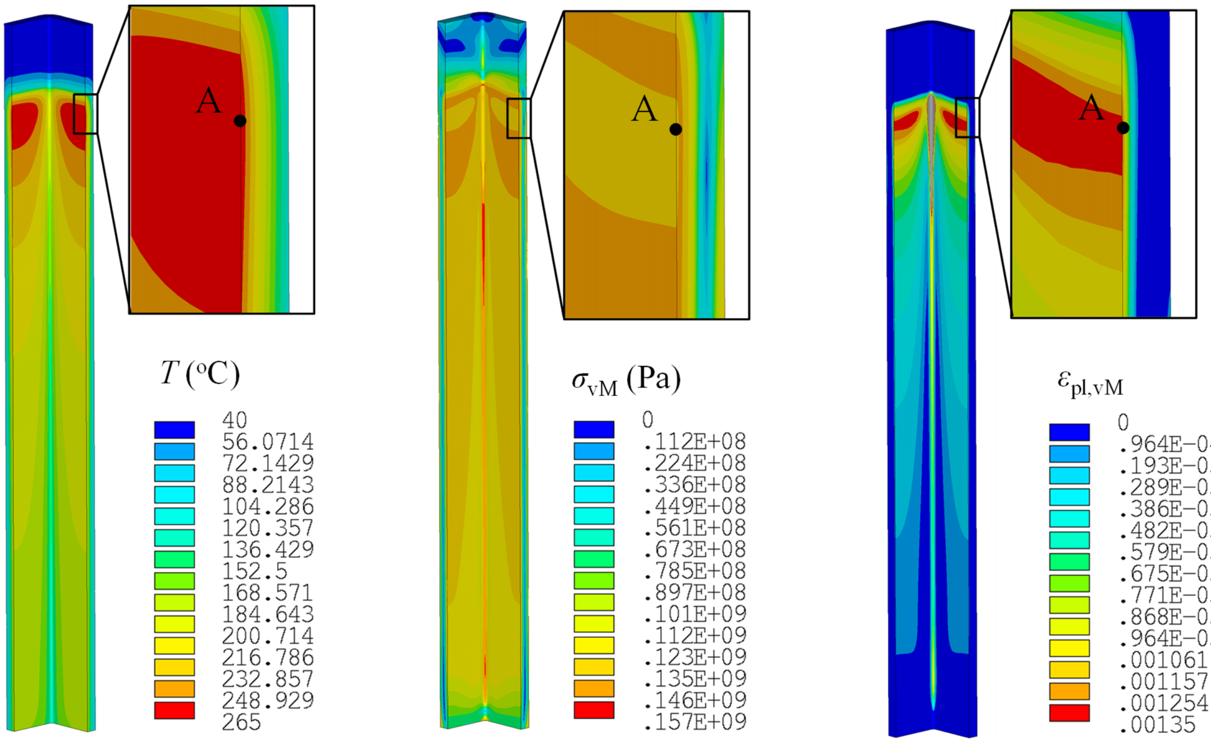

Fig. 12. Numerical model: a) temperature distribution at q_{max}, b) von Mises stress distribution, c) von Mises plastic strain distribution.

Fig. 13 and Fig. 14 present the through-thickness variation of the three stress components (hoop, axial and radial) calculated at point A, when the mold undergoes the thermal flux (*hot-phase*) and during the plant switch off due to maintenance (*cold-phase*), respectively. Hoop and radial components were parallel and perpendicular to the mold surface, respectively, whereas the axial component was along the mold axis. A biaxial state of stress occurred in the analyzed component. In the *hot* and *cold-phase*, both the hoop and axial stress followed a similar trend through the wall thickness, while the radial component was negligible. Indeed, once the plant has been switched on, the molten steel heats the inner part of the mold, whose temperature rapidly increases until the operating condition is fully reached (*hot-phase*). The outer part of the component is maintained at a lower temperature due to the presence of the cooling fluid. It follows that the inner hot portion of the mold tends to expand, but is constrained by the outer colder part. As a consequence, rather high compressive stresses occurred inside the mold and in the hottest area they even exceeded the material yield stress, see Fig. 13.

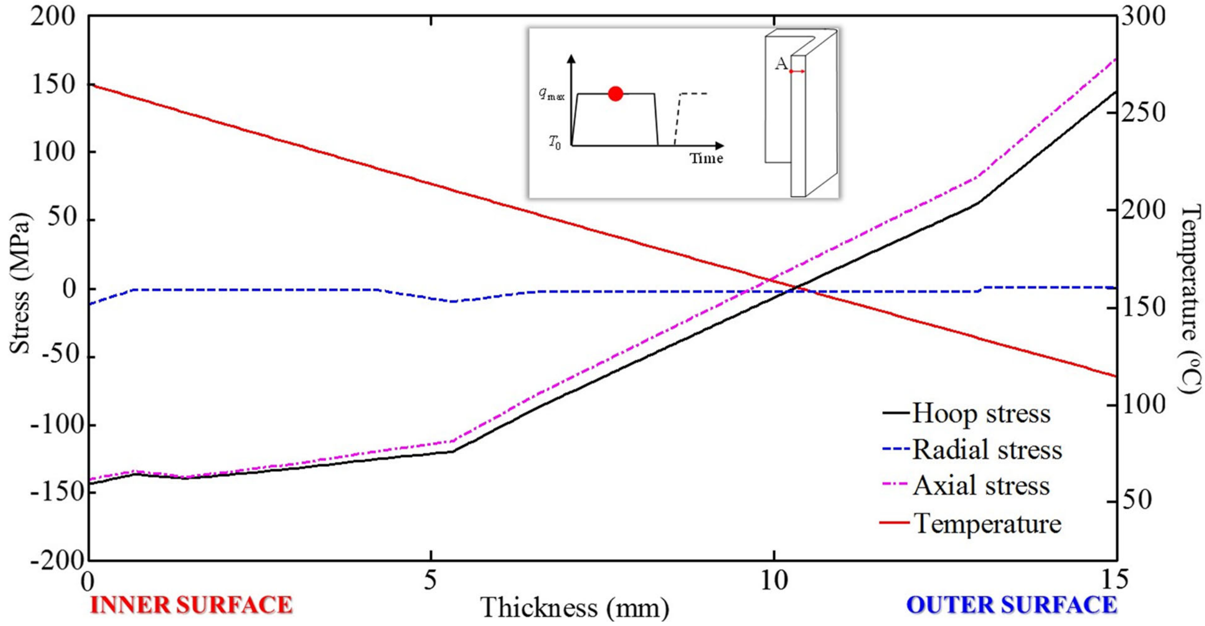

Fig. 13. Stress and temperature distribution versus thickness at the critical point A – *Hot-phase*.

The opposite occurs when the plant is switched off (*cold-phase*). In the latter case, the mold is cooled down to room temperature and consequently the zone plasticized during heating undergoes tensile stresses (Fig. 14).

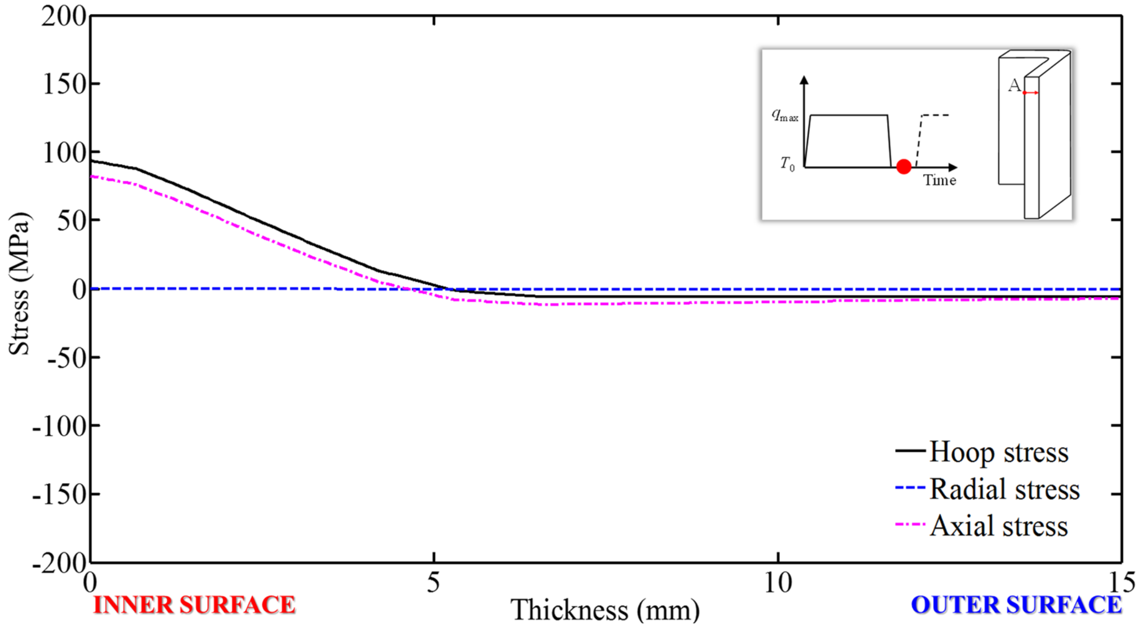

Fig. 14. Stress distribution versus thickness at the critical point A – *Cold-phase*.

4. Discussion

The experimental results showed that the damage mechanism of the copper mold was related to the synergistic effect of thermal fatigue and chemical/metallurgical degradation. This was confirmed by the visual inspection (Fig. 3a) which revealed severe damage close to the meniscus area, accompanied by the complete detachment of Cr coating. Indeed, the numerical analysis revealed the presence of high thermal stresses in the proximity of the meniscus area (Fig. 12) due the high thermal gradient reached in the *hot-phase*.

Owing to the plant being switched on/off continually, the stresses in the inner mold surface fluctuate from negative (compressive) values, approaching yielding, up to positive (tensile) values. These fluctuating stresses cause a thermal fatigue phenomenon, as demonstrated by several cracks mainly observed close to the meniscus area (i.e. in the position of sample A1 followed by A01), where temperatures are higher. According to O'Connor and Dantzig [8], the tensile stresses are responsible for damages that occur on the inner surface near the meniscus. Fig. 15 compares the inner surface of the real component and the distribution of the von Mises plastic strain, evaluated numerically in the same area. The most critical area (where the highest plastic strain values occur) is located where the cracks were observed with the metallurgical analysis.

Fig. 15. Comparison between the mold inner surface and the von Mises plastic strain distribution.

The experimental analyses of the damaged areas in the mold highlight that samples A1 and A01 were the most damaged. The SEM cross section analyses of the samples showed the presence of a Cu-Zn layer from which the cracks nucleated and then propagated in the Cu substrate. The Cr coating was completely detached in the meniscus area. The Cr detachment was the first damage that occurred in the Cu mold, which seems to be linked to the thermal fatigue to which the mold was subjected during the service life.

The difference in the thermal expansion coefficient between the Cu and the hard Cr coating [23] is the main cause of the coating failure. In this case, it is supposed that the highest stresses are located in the proximity of the interface between the substrate and the coating. Crack propagation as well as coating detachment are very rapid because, according to [24], micro-cracks already appear in an *as deposited* condition due to the brittle nature of the coating. As indicated by Hadavi *et al.* [14], the Cr coating undergoes a reduction of hardness during the high temperature exposure that lowers the mechanical properties (hardness, fatigue). The failure of the coating leads to an infiltration of low melting point elements (Zn, S, Pb), which are probably expelled during the solidification of the steel because of their low solubility or because they form low melting point compounds. These elements, which present a high affinity with Cu, infiltrate the cracks of Cr coating and generate a liquid metal infiltration, which presents a morphology similar to an undermining corrosion of the coating [2, 14, 21, 22, 25]. The coating is then detached and the bare Cu is exposed to the deleterious low melting point elements. In this case, the reaction of these elements with Cu is fast and controlled by the diffusion. In the meniscus zone, the Cu substrate reacts first with Zn, which forms brittle intermetallic phases (γ brass, β' brass or mixture of two). Furthermore, this brittle phase breaks, nucleating the thermal fatigue crack of the substrate, which propagates in the Cu alloy [2, 11]. The crack nucleation is intergranular (Fig. 9) and favored by the precipitation of intermetallic phases at grain boundaries. The crack propagation, instead, is transgranular (Fig. 10) and is enhanced by the infiltration of elements with a lower melting point temperature than Zn, as Pb and S (Fig. 5). In this case, probably because of the lower temperature inside the crack compared to the temperature of the internal wall of the mold, these elements infiltrate more in the crack than in the top surface. The result is a reaction of these elements with the Cu that produces brittle phases in the crack tip, which enhance the crack propagation of the thermal fatigue crack. The crack propagation in sample A1 was also favored by a possible grain growth of the Cu substrate that reduced locally the toughness of the material. The grain growth could be a consequence of the long time exposure of the material after the recrystallization process, as suggested by Barella *et al.* [11]. This was confirmed by both micro-hardness results and the metallographical investigation of the material. On the other hand, the specimen extracted from the corner presented the same degradation mechanism as the sample extracted from the meniscus area although it seemed to be exposed to less invasive thermo-mechanical damage (Fig. 5, Fig. 6 and Fig. 8).

The numerical thermal analysis identified the corners as the regions at the meniscus level that experienced a lower temperature (Fig. 12). Instead, specimens B1 and C1 (extracted in the areas away from the meniscus zone and exposed to the lower temperatures) showed a lower kinetics of infiltration (Fig. 7 and Tab. 4). This phenomenon is still present and linked to elements with a lower melting temperature than Zn (mainly S). The specimens D1 extracted from the coldest zone of the mold revealed the thermal fatigue cracking mechanism of the Cr coating quite clearly. In this case, because of the lower temperatures and the slowest infiltration of low melting point elements, the degradation mechanism was not completely developed as in the samples extracted from the meniscus.

5. Conclusions

The present work investigated the degradation mechanisms of a continuous casting mold after service. The experimental results showed that the meniscus area, which is the most stressed region of the mold, was heavily damaged by a thermo-mechanical degradation assisted by a chemical attack of the underlying material. In the early damage phase, degradation involves the complete detachment of the Cr coating used to protect the substrate underneath. Subsequent degradation is due to the liquid metal infiltration of low-melting point elements that embrittle the substrate directly exposed to the molten steel. These elements make thermal fatigue cracks nucleate and then propagate in the most critical area evidenced by FEM simulation in term of the most stressed locations.

Alternative coatings to the hard chromium plating (e.g. thermal spray coatings, binary/ternary alloys deposited by electrodeposition) could be adopted in order to delay the coating detachment and thus increase the mold service life. It would also be beneficial to decrease the amount of low melting point elements in the steel.

Acknowledgements

The authors are grateful to Prof. L. Fedrizzi, head of the material lab, for helpful comments, and to Mr. M. Magnan for technical support during the experimental analyses.

References

1 Park, J.K., Thomas, B.G., Samarasekera, I.V., Yoon, U.S. (2002) Thermal and mechanical behavior of copper molds during thin-slab casting (I): plant trial and mathematical modeling, *Metallurgical and Materials Transactions B*, **33B,** 1-12.

2 Park, J.K., Thomas, B.G., Samarasekera, I.V., Yoon, U.S. (2002) Thermal and mechanical behaviour of copper molds during thin slab casting(II): Mold crack formation, *Metallurgical and Materials Transactions B*, **33B**, 437-449.

3 Thomas, B.G. (2001) Continuous Casting of Steel. Chapter 15 in Modeling for casting and solidification processing, Dekker, M. (Ed.), New York, 499-540.

4 Srnec Novak, J., Stanojevic, A., Benasciutti, D., De Bona F. and Huter, P. (2015) Thermo-mechanical finite element simulation and fatigue life assessment of a copper mould for continuous casting of steel, *Procedia Engineering*, **133**, 688–697.

5 Moro, L., Srnec Novak, J., Benasciutti, D., De Bona, F. (2017) Copper mold for continuous casting of steel: Modelling strategies to assess thermal distortion and durability, *Key Engineering Materials*, **754,** 287-290, DOI:10.4028/www.scientific.net/KEM.754.287.

6 Moro, L., Srnec Novak, J., Benasciutti, D., De Bona, F. (2017) Thermal distortion in copper moulds for continuous casting of steel: Numerical study on creep and plasticity effect, *Ironmaking and Steelmaking*, in press (DOI: 10.1080/03019233.2017.1371425).

7 Moro, L., Benasciutti, D., De Bona, F. (2017) Simplified numerical approach for the thermo-mechanical analysis of steelmaking components under cyclic loading: an anode for electric arc furnace, *Ironmaking and Steelmaking*, in press (DOI:10.1080/03019233.2017.1339482).

8 O'Connor, T.G., Dantzig, J.A. (1994) Modeling the thin-slab continuous-casting mold, *Metallurgical and Materials Transactions B*, **25B**, 443-457.

9 Benasciutti D., Srnec Novak J., Moro L., De Bona F., Stanojevic A. (2018) Experimental characterization of a CuAg alloy for thermo-mechanical applications. Part 1: Identifying parameters of non-linear plasticity models, *Fatigue & Fracture of Engineering Materials & Structures*, **41**, 1364-1377, DOI:10.1111/ff3.12783.

10 Benasciutti D., Srnec Novak J., Moro L., De Bona F. (2018) Experimental characterization of a CuAg alloy for thermo-mechanical applications. Part 2: design strain-life curves estimated via statistical analysis, *Fatigue & Fracture of Engineering Materials & Structures*, **41**, 1378-1388, DOI:10.1111/ff3.12781.

11 Barella, S., Gruttaduria, A., Mapelli, C., Mombelli, D. (2014) Investigation of failure and damage on a continuous casting copper mould, *Engineering Failure analysis*, **36**, 432-438.

12 Faries, F., Rawson, J., Rose, A., Bugdol, M. (1996) Mould coatings for continuously cast billet production, Technical steel research – Final Report.

13 Pandey, J. C., Raj M., Mishra, R., Tripathy, V.K., Bandyopadhuau N. (2008) Failure of nickel coating on a copper mold of a slab caster, *Journal of Failure Analysis and Prevention*, **8**, 3-11.

14 Hadavi, S.M.M., Zadaeh, A. A., Jamshidi, M.S. (2004) The effect of thermal fatigue on hardness of hard chromium electroplating, *Journal of Materials Processing Technology*, **147**, 385-388.
15 ASTM B 124 - B 124M (2008) Standard specification for copper and copper alloy forging rod, bar, and shapes.
16 Udayraj, Chakraborty, S., Ganguly, S., Chacko, E.Z., Ajmani, S.K. and Talukdar, P. (2017) Estimation of surface heat flux in continuous casting mould with limited measurement of temperature, *International Journal of Thermal Sciences*, **118,** 435-447.
17 Samarasekera, I.V. (1980) Thermal distortion of continuous casting mould, Thesis, The University of British Columbia, Vancouver, Canada.
18 Thomas, B.G., Li, G., Moitra, A. and Habing, D. (1997) Analysis of thermal and mechanical behavior of copper molds during continuous casting of steel slabs, 80^{th} Steelmaking Conference, Chicago, USA.
19 Srnec Novak, J., Benasciutti, D., De Bona, F., Stanojevic, A., De Luca, A. and Raffaglio, Y. (2016) Estimation of material parameters in nonlinear hardening plasticity models and strain life curves for CuAg alloy, IOP Conf. Series: *Materials Science and Engineering*, 119, 012020.
20 Lemaitre, J., Chaboche, J.L. (1990) Mechanics of solid material, Cambridge University Press, Cambridge.
2116 Davis, J.R. (2001) Copper and copper alloys, First edition, ASM International, Ohio.
22 Gravemann, H. J., Brown, I., Tapley, C.D. (1981) Continuous casting of steel, 2nd process technology conference, Chicago, IL, **2**, 23-25.
23 Various authors (1990) ASM Metal handbook vol2: Properties and selection: Non-ferrous alloys and special-purpose materials, First edition, ASM International, Ohio.
24 Cotell, C.M., Sprague, J.A., Smidt Jr, F.A. (1994) ASM Metal Handbook Vol. 5: Surface engineering, First edition, ASM International, Ohio.
25 Korb, L.J. and Olson, D.L. (1992) ASM Metal handbook Vol. 13: Corrosion, Fourth edition, ASM International, Ohio.

FIGURE CAPTIONS

Fig. 1. A mold under working conditions (half section) and axial thermal flux distribution when q=q_{max}.

Fig. 2. Variation of the thermal flux during the service life of a mold.

Fig. 3. Mold under investigation with damaged inner surface (a), positions of extracted samples (b).

Fig. 4. Finite element model.

Fig. 5. SEM analysis of samples A01, A1 in top view and cross section. The letters indicate the areas analyzed by EDXS.

Fig. 6. SEM analysis of samples B1, C1, D1 in top view and cross section. The letters indicate the areas analyzed by EDXS.

Fig. 7. Detail of the interface of sample C1 (circled area in Fig. 6).

Fig. 8. Microstructural characterization of the analyzed samples.

Fig. 9. Detail of the material surface that identifies the crack nucleation morphology. The black arrows indicate the intergranular features. The white circle indicates the intergranular fracture.

Fig. 10. Image of the crack extension in sample A1.

Fig. 11. Microhardness profiles for the tested specimens: a) complete profile, b) zoom of the hardness between 50-110 HV0.1 (square area of Fig. 11a).

Fig. 12. Numerical model: a) Temperature distribution at q_{max}, b) von Mises stress distribution, c) von Mises plastic strain distribution.

Fig. 13. Stress and temperature distribution versus thickness at of the critical point A – *Hot-phase*.

Fig. 14. Stress distribution versus thickness atof the critical point A – *Cold-phase*.

Fig. 15. Comparison between the mold inner surface and the von Mises plastic strain distribution.